Electrochemical non-enzymatic urea sensing using polyvinylpyrrolidine derived highly electrocatalytic NiCo2O4 nanowires

Sanjha Mangrio, Aneela Tahira, Ihsan Ali Mahar, Mehnaz Parveen, Ahmed Ali Hullio, Dildar Ali Solangi, Abid Khawaja, Muhammad Ali Bhatti, Zahoor Ahmed Ibupoto, Arfana Begum Mallah, et al.

Electrochemical non-enzymatic urea sensing using polyvinylpyrrolidine derived highly electrocatalytic $NiCo_2O_4$ nanowires

Sanjha Mangrio[1], Aneela Tahira[2*], Ihsan Ali Mahar[1], Mehnaz Parveen[1], Ahmed Ali Hullio[1], Dildar Ali Solangi[6], Abid Khawaja[1], Muhammad Ali Bhatti[8], Zahoor Ahmed Ibupoto[7], Arfana Begum Mallah[1], Ayman Nafady[4], Elmuez A. Dawi[5], Abd Al Karim Haj Ismail[5], Melanie Emo[3], Brigitte Vigolo[3], Zafar Hussain Ibupoto[1*]

[1]Institute of Chemistry, University of Sindh Jamshoro, 76080, Jamshoro, Sindh Pakistan.
[2]Institute of Chemistry, Shah Abdul Latif University, 66111, Khairpur Mirs, Sindh, Pakistan.
[3] Université de Lorraine, CNRS, IJL, F-54000 Nancy, France.
[4]Chemistry Department, College of Science, King Saud University, Riyadh, 11451, Saudi Arabia.
[5]Nonlinear Dynamics Research Centre (NDRC), Ajman University, Ajman P.O. Box 346, United Arab Emirates.
[6]Department of Pathology, Diagnostic Laboratory, Liaquat University of Medical and Health Sciences, Jamshoro, 76080, Sindh Pakistan.
[7]Faculty of Agricultural Engineering and Technology, PMAS-Arid Agriculture University, Rawalpindi, Pakistan.
[8]Centre of Environmental Sciences, University of Sindh Jamshoro, 76080, Jamshoro, Sindh Pakistan.

***Corresponding authors**:*

Aneela Tahira, ***Email:*** *aneela.tahira@salu.edu.pk*,

Zafar Hussain Ibupoto, ***Email*****:** *zaffar.ibhupoto@usindh.edu.pk*

Abstract

It is highly desirable to use non-enzymatic urea sensors in the clinical, biomedical, agricultural, and food industries. Thus, we have utilized polyvinyl-pyrrolidine (PVP) to tune the shape, particle and electrochemical properties of $NiCo_2O_4$ nanowires during hydrothermal processes. $NiCo_2O_4$ nanowires were investigated under alkaline conditions 0f 0.1M NaOH in relation to their electrochemical activity in detecting urea using PVP. $NiCo_2O_4$ nanowires were analyzed using different analytical techniques to determine their structure, chemical composition, and crystallinity. The PVP has strongly changed the morphology of $NiCo_2O_4$ from nanorod to thin nanowires with diameter of 150 nm to 250 nm and the grain size was also reduced. . A cubic phase crystal system displayed a typical spinel structure in $NiCo_2O_4$ nanowires. $NiCo_2O_4$ nanowires prepared with 50 mg of PVP show a wide linear range of urea concentrations between

1 mM and 16 mM with a limit of detection of 0.01mM. In addition to this, the stability, selectivity, and reproducibility of the experiment were all satisfactory. Consequently, $NiCo_2O_4$ nanowires may perform better because they have a smaller particle size, a smaller grain size, are exposed to more catalytic sites, and have a higher electrical conductivity. The newly developed $NiCo_2O_4$ nanowire-bussed enzyme-free sensor was also examined for practicality.

Keywords: $NiCo_2O_4$ nanowires, polyvinylpyrrolidine, urea, enzyme free sensor.

1. Introduction

A variety of health problems can be associated with abnormal levels of various compounds in the blood, including diabetes, cardiovascular disease, heart disease, cancer, kidney failure, liver disorders, chronic respiratory disease, and tuberculosis. As a result, maintaining a healthy lifestyle requires reducing blood components like cholesterol, uric acid, urea, and glucose [1, 2]. As an example, urea is produced by the liver and transported to the kidneys through the bloodstream. In the kidneys, the urea is released to be used in the metabolism of proteins. Humans have urea levels that range between 15 and 40 mg/dL at a physiological level. A high level of urea can cause life-threatening diseases such as ulcers, digestion problems, acid reflux, urinary tract blockages, renal failure, kidney dysfunction, shock, gastrointestinal bleeding, cancer, burns, and many more. A low urea level, however, can lead to hepatic nephritis, cachexia, and failure [3]. Furthermore, urea is widely used in dairy, food preservation, agriculture, and fisheries, which makes its determination crucial. It is estimated that the level of urea in milk varies between 18 and 40 mg/dL [4]. The presence of urea is also an important component of a variety of pharmaceutical products in which it is desirable to control the concentration of the compound. By-products of sewage contamination can cause urea to appear in groundwater or rivers. According to studies, high concentrations of urea are responsible for algae blooms [5-8]. It is therefore imperative to develop a method for measuring urea levels with high selectivity and sensitivity. A variety of conventional methods are available to detect urea, including infrared (IR) spectroscopy [9, 10], high performance liquid chromatography [11], nuclear magnetic resonance (NMR) [12], calorimetric methods [13], gas chromatography [14], fluorimetry [15], and chemiluminescence. It takes considerable time and effort to conduct these techniques, and samples must be pretreated before urea determination can take place. Additionally, certain substances, including uric acid, potassium, and sodium ions, interfere with

the measurement [16, 17]. The majority of these techniques are based on the detection of urea by enzymatic methods and are restricted by concerns regarding storage and stability. The advantages of electrochemical biosensors, on the other hand, are their affordability, speed, and high selectivity [18, 19]. Biosensors have demonstrated their capabilities in a range of fields, including defense, industry, food safety, environmental protection, drugs, pharmaceutical monitoring, disease biomarkers, and homeland security [20-25]. It is possible to use disposable biosensor chips directly without the need for pretreatment in highly complex matrices [26-29]. As an added benefit, simultaneous detection of multiple targets could result in a reduction in fabrication costs and sample volumes, allowing for automatic, selective, and accurate measurements to be made [30]. Moreover, the nanowires based materials have been investigated for the wide range of sensing applications owing to their high sensitivity and rapid electron communication [31-36]. A novel and attractive approach to the detection of analytes has been developed using enzyme free sensing, which has resulted in the development of efficient catalytic materials for this purpose. These materials include cobalt oxide [37, 38], tin oxide [39], nickel cobalt oxide [40], nickel/cobalt oxide graphene composite [41], and polypyrrole/platinum composites. $NiCo_2O_4$ exhibits significant electrical conductivity, catalytic activity, and rapid charge transport properties, making it an ideal material for sensing urea without enzymes [42-43]. It has been demonstrated that $NiCo_2O_4$ nanostructures can be synthesized by various methods, such as hydroxide decomposition [44], electrodeposition [45], co-precipitation [46], and solvothermal synthesis [47]. Using solvothermal methods for synthesis of $NiCo_2O_4$ nanostructures is one of the most promising approaches because it offers the possibility to kinetically control the growth of nanostructured materials as well as polymer-assisted synthesis. Orientation and size of nanostructures determine the final application of materials, which is largely dependent on their size. This means the size and morphology of crystals are affected by pressure, temperature, pH, and surfactants, all of which are critical parameters for tuning microstructures [48, 49-54]. Using polymer polyvinylpyrrolidone (PVP), $NiCo_2O_4$ nanostructures with rod-like shapes were prepared by co-precipitating cobalt and nickel oxalates salts by hydrothermal method [55, 56, 57].

Changing the shape, particle size, and electrical conductivity of $NiCo_2O_4$ nanostructures using PVP can tailor them for various electrochemical applications. Different PVP masses enable

$NiCo_2O_4$ nanostructures to electrochemically catalyze the detection of urea. Currently, no literature has been published on PVP's role in improving $NiCo_2O_4$ nanostructures' electrochemical activity for urea detection. The PVP exhibits surfactant-like properties, which changed the surface properties of $NiCo_2O_4$ nanostructures, and hence improved catalytic properties were observed. This study presents a detailed examination of the effects of different PVP masses on the electrochemical performance of $NiCo_2O_4$ nanostructures for the detection of urea. An electrochemical study of $NiCo_2O_4$ nanostructures found that PVP has a significant influence on its performance.

2. Materials and Methods

2.1. Chemical reagents

The following materials were purchased from Sigma Aldrich, Karachi, Sindh Pakistan: cobalt chloride hexahydrate, nickel chloride hexahydrate, urea, polyvinyl-pyrrolidine (10000 MW), ethanol, sodium hydroxide, glucose, uric acid, potassium chloride, and sodium chloride. In order to achieve the desired results, deionized water was used as a solvent.

2.2. Synthesis of $NiCo_2O_4$ nanowires oxide nanowires using PVP

To fabricate nanostructured bimetallic oxide nanowires, the solvothermal method was adapted. We dissolved 0.1 M cobalt chloride hexahydrate, 0.1 M urea, and 0.05 M nickel chloride hexahydrate in ethanol and deionized water. Water and ethanol were diluted 20:80 by volume. A Teflon vessel was filled with 100 mL of solution in the next step. The growth process was performed in an autoclave with a tight seal at 120 °C for five hours. Deionized water and ethanol were used to wash the product several times before it was allowed to dry overnight. Afterwards, they were heated to 400 °C in an atmosphere of air for 3 hours. A similar experiment added 50 mg of polyvinylpyrrolidine dissolved in 20 mL of ethanol to the above precursor concentration with a total volume of 100 mL. Different amounts of polyvinyl-pyrrolidine were used to evaluate whether polyvinyl-pyrrolidine affected the aspect ratio of $NiCo_2O_4$ nanowires. As softening and sacrificing agents, 50 mg (sample 1) and 100 mg (sample 2) polyvinylpyrrolidine were dissolved

in 20 mL of ethanol separately. Scheme 1 describes the synthesis of $NiCo_2O_4$ nanowires using different PVP amounts.

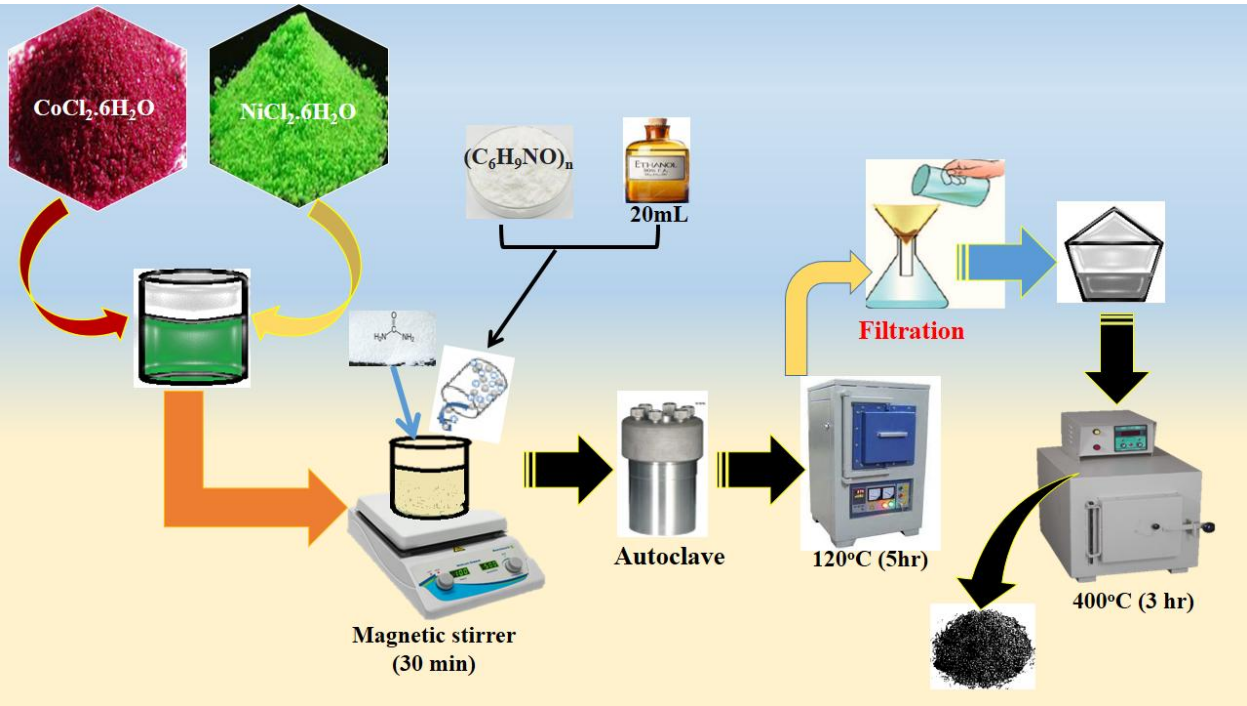

Scheme 1: Synthesis process of $NiCo_2O_4$ nanowires using PVP by solvothermal method.

2.3. Structural and crystalline characterizations

The shape structure, crystal quality, and chemical composition of the sample were examined using different analytical instruments. A ZEISS Gemini SEM 500 equipped with a field emission gun at a voltage of 15 kV was used for scanning electron microscope (SEM) observations. Powder X-ray diffraction (XRD) using Cu Kα radiation (Cu $\lambda K\alpha = 1.5406$ Å) and high resolution transmission electron microscope (HRTEM) (JEOL, JEM-ARM 200F) operating at 200 kV and equipped with Energy X-ray Dispersive Spectroscopy (EDXS) detector (SDD, Joel DRY SD 30 GV). An ethanol dispersion of the powder samples was deposited as a droplet on a holey carbon grid (200 mesh). With the help of a spectrophotometer (4100, JASCO), the different functional groups were measured through Fourier transform infrared (FTIR) spectra. An electrochemical experiment was conducted on Versa potentiostat.

There are three electrode configurations in the electrochemical cell, namely silver-silver chloride (Ag/AgCl, 3.0 M KCl), platinum sheet electrodes, and glassy carbon electrodes modified with $NiCo_2O_4$ nanostructures as reference electrodes, counter electrodes, and working electrodes. The GCE was washed and cleaned using a paste of alumina (0.3μM) and deionized water. An aqueous slurry of $NiCo_2O_4$ nanostructures and 5% Nafion was prepared by combining 5 mg of the nanostructures with 2.5 mL of deionized water and 0.2 mL of Nafion. A drop cast method was employed to deposit the $NiCo_2O_4$ nanostructure slurry onto the cleaned GCE. After drying for 15 minutes with air, the slurry was ready to be tested electrochemically. A fresh solution of urea in sodium hydroxide was prepared and non-enzymatic measurements were performed in an alkaline solution of 0.1M NaOH.

3. Results and discussion

3.1. Structural and crystalline property investigations of various samples of $NiCo_2O_4$ nanostructures

According to Figure 1, morphological features of $NiCo_2O_4$ nanostructures were examined using SEM in different amounts of PVP. Fig. 1a shows the comparison between $NiCo_2O_4$ nanostructures prepared with PVP and $NiCo_2O_4$ nanostructures prepared without PVP. $NiCo_2O_4$ nanostructures were shown to possess platelet-like morphologies containing assembled nanoparticles. However, when using 50 mg and 100 mg of PVP as morphology orienting agents, thinner nanowires are formed, as shown in Figures 1b and 1c. Figures 1b and 1c illustrate the dimensions of $NiCo_2O_4$ nanowires oriented in PVP with an average diameter between 150 and 250 nanometers, more than 2 times thinner than that of $NiCo_2O_4$ structures prepared without PVP. PVP's capping agent properties may influence $NiCo_2O_4$ nanostructures' size and shape orientation due to its tendency to bind to metal ions and create reduced morphologies. This effect was characterized by greater PVP mass during $NiCo_2O_4$ nanostructure growth. Nanostructured materials have previously been grown with PVP and similar observations have been reported [58, 59, 60]. A crystal quality analysis was performed using powder XRD as shown in figure 1d. The crystalline properties of $NiCo_2O_4$ nanostructures were significantly improved with increasing PVP amounts based on Figure 1d. The diffraction patterns of $NiCo_2O_4$ nanostructures

were observed at two angles: (111), (220), (331), (222), (400), (422), (511), and (440). These Miller indices indicate that $NiCo_2O_4$ nanostructures have a spinel structure and cubic phase that are similar to the standard JCPDS card 01-073-1704. The addition of PVP enabled us to obtain very intense reflections and verify the material's quality. In an XRD analysis, NiCo2O4 nanostructures prepared with different masses of PVP were found to be highly pure and to be free of any other contaminants.

$NiCo_2O_4$ nanostructures prepared with or without PVP have been characterized by TEM, HRTEM, and EDXS in terms of morphology, crystalline structure, and chemical composition; Figure 2. The morphology of pure $NiCo_2O_4$ nanostructures is nanorod-like (Figure 2a), and Ni, Co, and O make up their chemical composition. As shown in Figure 2e, $NiCo_2O_4$ prepared with PVP displays similar morphology, but grains of a different shape and smaller size were also noticed (Figure 2f). In a similar fashion to pure $NiCo_2O_4$, EDX analysis reveals that these particles are composed primarily of nickel, cobalt, and oxygen, but chlorine was identified as one of the impurities (Figure 2h). HRTEM results (Figures 2c, 2g) demonstrate that $NiCo_2O_4$ nanostructures with or without PVP exhibit a cubic crystal structure (Fd-3m, a = 8,1 Å), as supported by measured XRD patterns.

Figure 3 shows FTIR results for $NiCo_2O_4$ samples prepared under various chemical environments, such as urea concentration and PVP concentration. Different bands were observed for $NiCo_2O_4$ samples synthesized using different amounts of urea, including 564, 655, 783, 874, 1036, 1120, 1156, 1286, 1313, 1404, 1468, 1617, 1696, 1747, 2851, 2929, and 3427 cm^{-1}. The stretching vibrations of metal oxide and spinel chemical compounds range from 400 to 700 cm^{-1}, in our case, notable band counts of 564 and 655 cm^{-1} could apparently be associated with Ni-O and Co-O stretching bands for spinel structures of various $NiCo_2O_4$ samples [58]. On the surface of various $NiCo_2O_4$ samples, the band located at 3427 cm^{-1} is associated with the hydroxyl molecule, while the band located at 1617 cm^{-1} is associated with the bending vibrations of the molecules [58]. C-H stretching vibrations were detected at 2851 and 2929 cm^{-1}, respectively. It would be possible to label the stretching vibration at 1617 cm^{-1} to a typical carbonyl group. Stretching and bending vibrations in the range of 1036 to 1468 cm^{-1} are classified as N-H, O-H, and other vibrations. FTIR analysis of various samples of $NiCo_2O_4$ produced using different

amounts of PVP revealed that wet chemically synthesized $NiCo_2O_4$ could be successfully synthesized using various compositions of PVP.

3.2. Non-enzymatic urea sensing performance evaluation of PVP assisted synthesis of $NiCo_2O_4$ nanostructures

A brief electrochemical configuration of non-enzymatic urea based on PVP derived $NiCo_2O_4$ nanostructures is shown in Scheme 2.

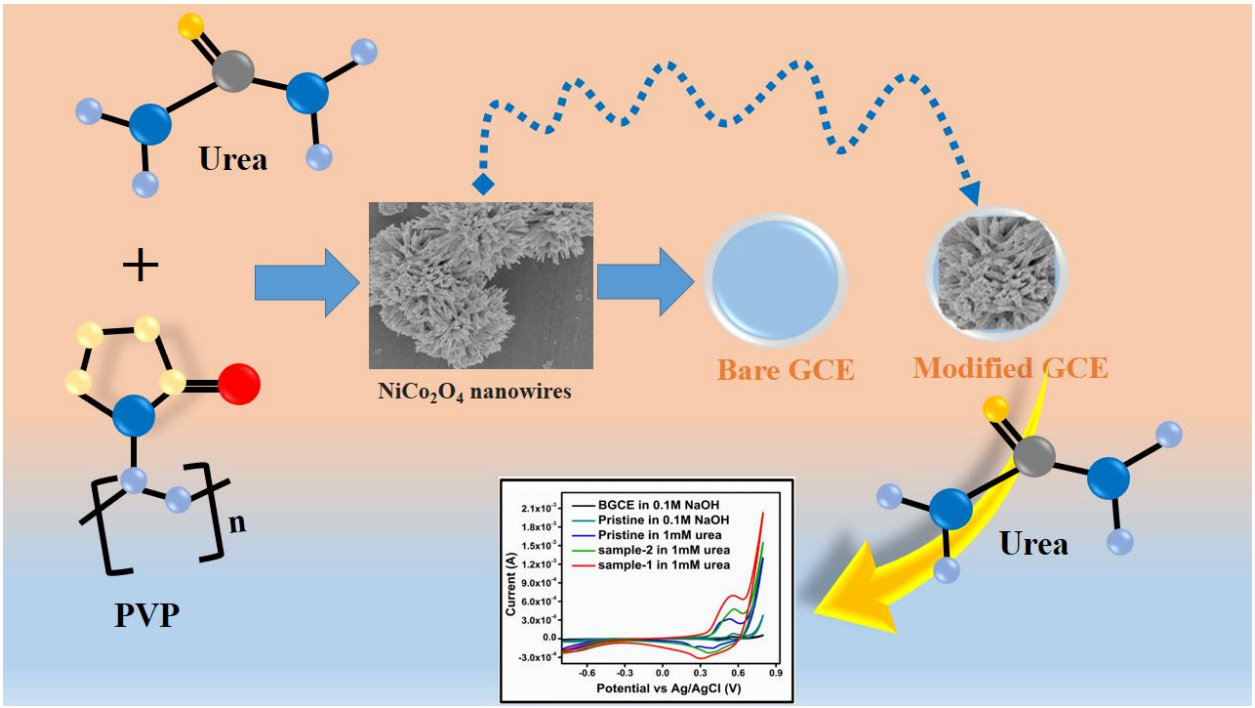

Scheme 2: Generalized presentation of electrochemical sensing of urea onto PVP derived $NiCo_2O_4$ nanostructures

A cyclic voltammetry as the primary electrode mode has been used to evaluate the effect of PVP on the electrochemical performance of $NiCo_2O_4$ nanostructures for the enzyme-free detection of urea. In Figure 4, CV scans were measured for a variety of $NiCo_2O_4$ nanostructures. The CV curves of all newly prepared materials were examined in 0.1 M NaOH with and without urea. During the CV study, pristine $NiCo_2O_4$ nanostructures exhibited good redox properties in the

electrolyte and relatively better redox properties in urea solution at 1 mM. Alternatively, $NiCo_2O_4$ nanostructures used for enzyme-free urea sensing have improved their redox properties when exposed to PVP. Based on this study, it was determined that 50 mg of PVP is an optimal amount of PVP for enhancing $NiCo_2O_4$ nanostructure electrochemical activity.

Nanostructures of $NiCo_2O_4$ prepared robotically (sample 1) showed improved redox properties when compared to those prepared with 100 mg of PVP (sample 2). The $NiCo_2O_4$ nanostructures prepared with 100 mg, however, perform even better electrochemically for urea detection than pristine $NiCo_2O_4$ nanostructures. From CV analysis as shown in Figure 4 about the oxidation of urea, we have witnessed that the different morphologies of $NiCo_2O_4$ has shown great impact on the kinetics of urea oxidation. The pure $NiCo_2O_4$ possessed the nanorod like shape which possibly showed less number of catalytic sites during the urea oxidation, hence limited the rate of urea oxidation was noticed, while the $NiCo_2O_4$ nanowires with less quantity of PVP (sample 1) has demonstrated the efficient oxidation peak current, suggested that nanowires were well oriented and exposed the maximum catalytic sites for the urea oxidation, hence highly sensitivity signal was noticed. Further, the $NiCo_2O_4$ nanowires obtained with higher quantity of PVP (sample 2) might show the large coverage of catalytic sites, consequently less exposure to the urea molecules for the oxidation. It could be illustrated from the CV analysis shown in Figure 4 that morphology of $NiCo_2O_4$ has great influence on the reaction kinetics of urea. CV analysis revealed that sample 1 was the optimal $NiCo_2O_4$ nanostructures with PVP for full sensing characterization. A variety of sensing parameters were measured on sample 1, including scanning rate, linear range, stability, reproducibility, selectivity, and real-time analysis of the sample.

As can be seen in Figure 5a, we investigated the electrode kinetics of sample 1 through CV studies at various scan rates in urea solution at a concentration of 1 mM. Based on the measured CV curves, it is evident that redox features are evident, which indicate reversible properties. Several redox properties can be reversed depending on the Ni^{2+}/Ni^{3+} ratio [59]. Interestingly, the CV curve shows $Ni(OH)_2$ being transformed into NiOOH in the forward direction, while the backward scan will show oxidized NiOOH being reduced and the active sites for urea oxidation being regenerated. Based on the CV curves measured at each scan rate in Figure 5a, the oxidation peak current increases linearly as the scan rate increases. On the basis of CV curves recorded at different

scan rates, Figure 5b illustrates how oxidation and reduction peak currents are plotted against square root of scan rate. The scan rate analysis suggests that the peak current was successively increasing with the increasing sweeping rate and built a linear correlation through a linear regression coefficient of 0.99. As shown by [60], the forward scan rate is associated with the oxidation of urea into nitrogen and carbon monoxide, whereas the reverse scan rate is associated with regeneration of active sites. In general, this is characterized by the following chemical equations:

$$6NiO + 6OH^{-} \rightarrow 6NiOOH + 6e^{-} \quad (1)$$

$$6NiOOH + CO(NH_2)_2 + 2OH^{-} \rightarrow 6Ni(OH)_2 + N_2 + CO_3^{2-} \quad (2)$$

$$CO(NH_2)_2 + 6OH^{-} \rightarrow N_2 + 5H_2O + CO_2 + 6e^{-} \quad (3)$$

Based on the linearly fitted scan results with regression coefficients of 0.99 for both forward and reverse scans, the results suggest that the diffusion-controlled mass transport on the surface of sample 1 contributes to the detection of urea.

The use PVP was taken into consideration for the tuning the particle size, shape, and electrochemical properties for the sensitive non-enzymatic detection of urea. The synthesis of $NiCo_2O_4$ nanowires using PVP was highly influenced through the strong interaction of amide groups of PVP polymeric chains with the metal ions via [61]. It has been shown that PVP stabilizes the nanostructures via steric and electrostatic effects created by the amide groups of pyrrolidine rings and alky groups. The metal ions are capped by the adsorption of short range polymeric chains which are produced during the beginning of hydrothermal reaction [62]. It has been observed that the effect of PVP could into be ignored during the calcination process wherein the smaller particles agglomerate, thus bigger particles formation takes place due to higher energy levels of smaller particles via Ostwald ripening phenomenon [63, 64]. These aspects during the calcination have been contributed from the larger molecular weight chains and repulsive forces operating within the polyvinyl group [65, 66]. These type of observations have been reported previously by the scientific community [67, 68, 69]. This illustrates that the particle size is highly influenced by the use of PVP which is greatly noticed from the presented SEM, TEM and XRD results. These precious studies highlighted the attractive PVP aspects including capping, stabilizing and surface modifying agents and they together changed the

surface properties of $NiCo_2O_4$ nanowires in terms of catalytic sites. Thus, these catalytic properties of surface modified $NiCo_2O_4$ nanowires were well capitalized during urea detection which could be seen from the CV curves with respect to enhanced oxidation peak current. Hence, the particle size, shape orientation and modified surface properties of $NiCo_2O_4$ nanowires played a vital role for the sensitive detection of urea.

3.3. Investigations of urea non-enzymatic sensing parameters of proposed $NiCo_2O_4$ nanostructures

A CV measurement in 0.1 M NaOH aqueous solution was used to estimate the urea sensor's limit of detection (LOD), limit of quantification (LOQ), and linear range using $NiCo_2O_4$ nanostructures (sample 1). Various urea concentrations were tested using CV tests at 50 mV/sec. In Figure 6a, the peak oxidation current was linearly related to the urea concentration (up to 16 mM). Based on these sensor characteristics, sample 1 exhibits strong electrocatalytic properties that are enhanced by PVP. In this way, PVP helps enhance the electrochemical properties of $NiCo_2O_4$ nanostructures by acting as a capping agent, a structure directing agent, and a particle size decrease agent. Figure 6a illustrates how this exposure led to efficient urea oxidation under alkaline conditions. In Figure 6b, a linear plot relating urea concentrations to oxidation peak current was constructed, and a regression coefficient of 0.99 was obtained for the range of 1 mM to 16 mM, demonstrating the excellent analytical features of sample 1. Using chronoamperometry at an applied potential of 0.57 V, we also assessed the linear range of our proposed sensor configuration. We noticed few challenges about the characterization of $NiCo_2O_4$ nanowires such as urea detection above 16 mM range as the electrical signal of nanowires was saturated due to full exploitation of catalytic sites. Hence, the full control on the length and diameter of diameter of nanowire is highly desirable as we used the hydrothermal process where it was difficult to control on the uniform length and diameter of nanowires, therefore more studies are required on this aspect. Figure 7a illustrates highly linear amperometric results between 1 mM and 11 mM. In response to an increase in concentration, current has also increased significantly. The sensor's response time was extremely fast and the signal became extremely stable for each concentration of urea for the short interval of time. Figure 7b shows the linear plot was estimated by selecting the measured current of the

amperometric curve under the stable area response time curve. This was done for a variety of urea concentrations. The $NiCo_2O_4$ nanowires exhibited the surface to volume ratio and offered the large surface for the adsorption of urea molecules thereby catalytic sites might play a vital role for the rapid oxidation of urea, thus an enhanced sensitivity was observed.

In the previous study [70], equations 4 and 5 were used to calculate LOD and LOQ. The slope after the linear plot is defined as m, whereas the standard deviation is defined as:

$$\text{LOD} = 3\ S/m \quad (4)$$

$$\text{LOQ} = 10\ S/m \quad (5)$$

The presented urea sensor resulted in LOD and LOQ values of 0.01 mM and 0.12 mM, respectively. Urea detection is highly sensitive due to PVP's ability to reduce particle size, grain size, and enhance electrical conductivity, resulting in highly sensitive electrical signals. A comparison was made between the performance of sample 1 for enzyme free detection of urea and that reported in previous publications. Using PVP, it was shown in this study that non-enzymatic urea sensors were greatly enhanced in sensitivity and the results obtained were superior to those obtained using enzyme-free methods [70]. A study of the stability of sample 1 in 1 mM of urea concentration is shown in Figure 8a. It is shown in Figure 8a that the oxidation peak current and oxidation potential did not change during the continuous repeatable CV cycle. The relative standard deviation was less than 3% for 18 CV cycles, indicating high stability. Among the competitive parameters for developing non-enzymatic urea sensors is their selectivity under the microenvironment of common interfering agents. In Figure 8b, we demonstrate how sodium, potassium, uric acid, and glucose are successively added to 1 mM urea solution to reach this objective. Interfering substances added sequentially at 0.1 mM concentrations did not alter the amperometric response. It can be concluded from the selective response results that the nanostructured material in sample 1 is only responsive to urea. It can be utilized as an alternative electrode material for the enzyme-free detection of urea. The selectivity of $NiCo_2O_4$ nanowires could be assigned to the use of PVP which tuned the surface and may only supported the favorable selectivity of urea sensor. The unique $NiCo_2O_4$ nanowires physiochemical properties such small size, modified surface and well orientation could play a vital role towards highly selective response for urea even in the presence of potential interfering agents. Furthermore, we tested the $NiCo_2O_4$ nanowires under the potential interfering agents with successive addition of each interfering agent

inside the reaction cell set up of urea solution. It did not show any change in the electrical signal, while the each successive addition also created the complex environment despite that the sensor signal was unaffected. The point of care of using non-enzymatic approach of sensing is about the design of the catalytic material which can only respond to the specific analyte. The presented $NiCo_2O_4$ nanowires were prepared with PVP, taking into view the amide groups which potential tuned the surface features of the material and enabled it towards the selective urea detection. We did not experience any issue during the selectivity test, however we believe that the more studies are required considering the higher concentrations of interfering agents. And the full characterization of selectivity of non-enzyamtci sensors should be carried out under the complete microenvironment of real world systems. These aspects should be taken into observations for the future studies.

As shown in Figure 8c, stability measurements through repeatable CV cycles can simplify understanding electrochemical signal variation On the basis of the bar graph with error bars, it appears that the peak current variation is negligible with continuous repeatable CV cycles; thus, the electrode material can be used for long-term urea detection. In addition, we have evaluated the linear range and limit of detection for the CV experiment to demonstrate the storage life of the modified electrodes at different intervals as shown in Table 1. These results indicate that the urea sensor presented is capable of maintaining linear range and limit of detection for three weeks with negligible variation in these parameters.

The urea sensor configuration was evaluated in real samples by using a standard addition method and percent recovery method to detect urea in milk and blood samples. Table 2 presents the results of real sample analysis performed three times with statistics deviation. As shown in Table 2, real-time urea detection demonstrated high reliability and accuracy with a relative standard deviation of less than 1%. A relative standard deviation (RSD) was estimated using the formula (standard deviation/mean of measured urea concentration over three repeated measurements) ×100%. The purpose of the presented study was to design an alternative urea sensor which can detect urea practically from the dairy products like milk and blood samples. From this perspective, the linear range experienced by the presented non-enzymatic urea sensor was found in the desired range and it was successfully evaluated during the real sample analysis. This conformed the practicality of our presented non-enzyamtci urea sensor under these conditions. For the wide linear range and low

level detection of urea using nanowire morphology, we need to produce the well-controlled nanowires in terms of length and diameter, then possibly we can encounter the urea detection at the wide linear range and low limit of detection.

In addition, Table 3 compares the electrochemical urea sensor with recently reported non-enzymatic urea sensors. As shown in Table 3, the proposed urea configuration is associated with a wide linear range, a limited detection limit, and simple and scalable synthesis of sensing material [71-75]. Consequently, the presented non-enzymatic urea sensor can be used for detecting urea in a variety of real-life samples as an alternative and efficient method. Moreover, our strategy about the synthesis of $NiCo_2O_4$ nanowires in the presence of PVP was relatively facile, low cost, properly oriented nanowires, rich catalytic sites and enhanced electrical conductivity compared to the previous works published works as given in Table 3. These are the few aspects which are highly desirable from the synthetic point of view about the detection of urea. Hence, such goals were successfully achieved. From the sensor performance point of view, the non-enzymatic urea sensing of many of the reported works is limited by the poor sensitivity and selectivity. Whereas, the presented urea sensor has shown better performance in terms of enhanced sensitivity and selectivity compared to the previous studies owing to the use of PVP which tuned the particle size, surface properties and morphology of $NiCo_2O_4$ nanowires.

Table 1: Life time of as proposed non-enzymatic urea sensor based on PVP derived $NiCo_2O_4$ nanostructures.

Number of days	Linear range (mM)	Limit of detection (mM)	(%)RSD
7	1-16± 0.002	0.01± 0.003	0.35
14	0.95-16± 0.004	0.02± 0.005	0.42
21	0.99-15.97± 0.005	0.012± 0.004	0.51

Table 2: Real sample analysis of 50 mg PVP derived $NiCo_2O_4$ nanostructures towards urea detection using % recovery method.

Sample ID	Added (mM)	Found (mM)	(%) Recovery	(%) RSD
Milk 1	----	1.8	---	
---	0.5	2.31 ± 0.003	100.43	0.39
	1	3.29 ± 0.001	99.69	0.41
	1.5	4.82 ± 0.002	100.41	0.40
Milk 2	-----	2.4	----	
	1	3.39 ± 0.001	99.70	0.51
	1.5	4.92 ± 0.002	100.40	0.49
	2	9.88 ± 0.001	99.71	0.48
Blood 1	----	4.4	-----	
	0.5	4.91 ± 0.002	100.20	0.58
	1	5.93 ± 0.003	100.50	0.55
	2	7.87 ± 0.001	99.60	0.57
Blood 2	------	5.2	---	
	1	6.22 ± 0.003	100.32	0.44
	1.5	7.68 ± 0.001	99.74	0.42
	2	9.73 ± 0.004	100.30	0.41

Table 3: Comparison of performance of proposed electrochemical urea sensor with recently reported urea biosensors.

Sensing material	Linear range (mM)	Limit of detection (mM)	Method of detection	References
$Ni(OH)_2/Mn_3O_4$/ rGO/PANi	0.03–3.3	0.0163	Non-enzymatic	71
$NiO–MoO_3$	0.2–1	0.086	Non-enzymatic	72
(Ni-MOF) nanobelts	0.01–7.0	0.0223	Non-enzymatic	73
$NiCo_2O_4$	0.01-5	0.01	Non-enzymatic	74
NF-LDH	0.5 to 8 mM	0.114 mM	Non-enzymatic	75
$NiCo_2O_4$ nanowire	1-16 mM	0.01	Non-enzymatic	**Present Work**

4. Conclusions

$NiCo_2O_4$ nanostructures were hydrothermally grown using PVP as a surface modification and sacrificing agent. The electrochemical properties of $NiCo_2O_4$ nanostructures, as synthesized, were examined by using PVP to detect urea by nonenzymatic means in a 0.1M aqueous solution of NaOH. Nanorods of $NiCo_2O_4$ nanostructures were transformed into nanowires by PVP, resulting in decreased grain and particle sizes. $NiCo_2O_4$ nanostructures prepared with PVP had also altered their surface properties, as shown by their electrochemical performance for the detection of urea. A urea sensor configuration prepared from $NiCo_2O_4$ nanostructures with 50 mg of PVP (sample 1) demonstrated a linear range of 1 mM to 16 mM in CV mode, and 1 mM to 11 mM in chronoamperometry mode. In addition, a low detection limit of 0.01mM and low quantification limit of 0.12 mM were found to be associated with the proposed urea sensor. Sample 1 was highly stable, sensitive, reproducible, repeatable, and selective during urea sensing. Analyses of real samples have been performed successfully with the urea sensor presented here. A surface-modifying and surface-sacrificing agent such as PVP can be used for developing advanced biomedical devices based on the results obtained.

Acknowledgment

The authors would like to acknowledge the Higher Education Commission of Pakistan for its partial support of the project (NRPU/8350). The authors extend their sincere appreciation to the Researchers Supporting Project number (RSP2023R79), King Saud University, Riyadh, Saudi Arabia, for partial funding of this work. The authors acknowledge partial funding from Ajman University, Grant DRGS Ref: 2022-IRG-HBS-5. Brigitte Vigolo and Mélanie Emo would like to thank the platform “Microscopies, Microprobes and Metallography (3 M)” (Institut Jean Lamour, IJL, Nancy, France) for access to TEM and SEM facilities.

Conflicts of Interest

Authors have no conflict of interest in the presented research work.

Funding Declaration

Not Applicable.

Data Availability Statement

The authors declare that the data supporting the findings of this study are available within the paper.

Author's contributions

Sanjha Mangrio, performed synthesis of nanostructured materials and involved in the electrochemical measurements.

Aneela Tahira, performed XRD analysis and wrote the draft.

Ihsan Ali Mahar, performed partial electrochemical analysis.

Mehnaz Parveen, performed partial electrochemical investigations.

Ahmed Ali Hullio, performed pre-review of the paper.

Dildar Ali Solangi, involved in real sample collection and preparation.

Abid Khawaja, performed real sample analysis.

Muhammad Ali Bhatti, performed overall presentation of data and edited the draft.

Zahoor Ahmed Ibupoto, performed FTIR measurement and analyzed the results

Arfana Begum Mallah, performed partial supervision.

Ayman Nafady, performed proofread of the paper and validated the results.

Elmuez A. Dawi, provided the concept and edited the draft.

Abd Al Karim Haj Ismail, verified the electrochemical results.

Melanie Emo, performed HRTEM analysis .

Brigitte Vigolo, performed SEM analysis and corrected the draft.

Zafar Hussain Ibupoto, performed main supervision and wrote the first draft of manuscript.

Figures

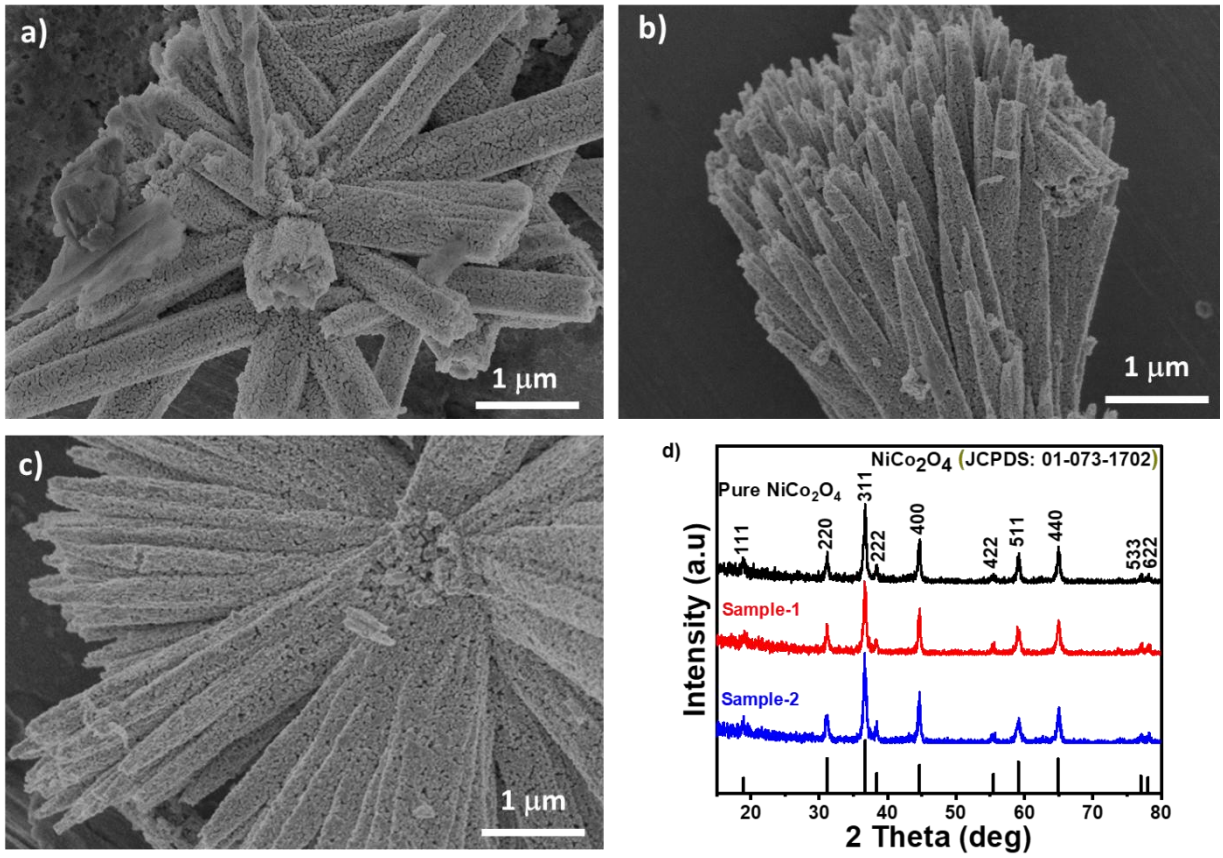

Figure 1. Typical SEM images of a) pure $NiCo_2O_4$ nanostructures, b) $NiCo_2O_4$ nanowires prepared with 50 mg of PVP (sample 1) and c) $NiCo_2O_4$ nanowires prepared with 100 mg of PVP (sample 2), (d) XRD diffraction patterns of pure $NiCo_2O_4$ nanostructures and PVP assisted $NiCo_2O_4$ nanowires (sample 1 and sample 2).

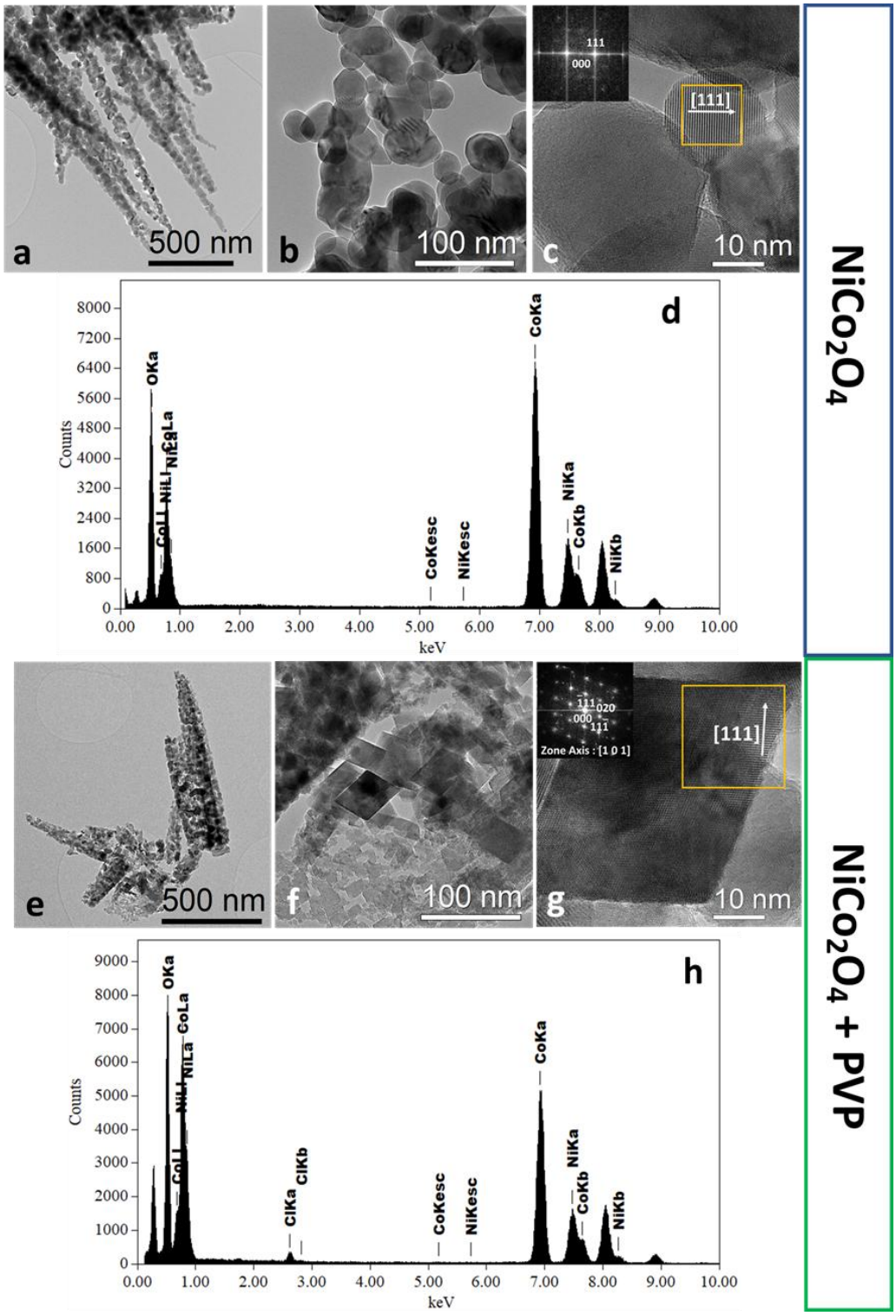

Figure 2. TEM micrographs of pure $NiCo_2O_4$ (a-b) and sample 1 (e-f) nanostructures, HRTEM micrographs of pure $NiCo_2O_4$ (c) and sample 1 (g) nanostructures and corresponding EDX spectra (d, h).

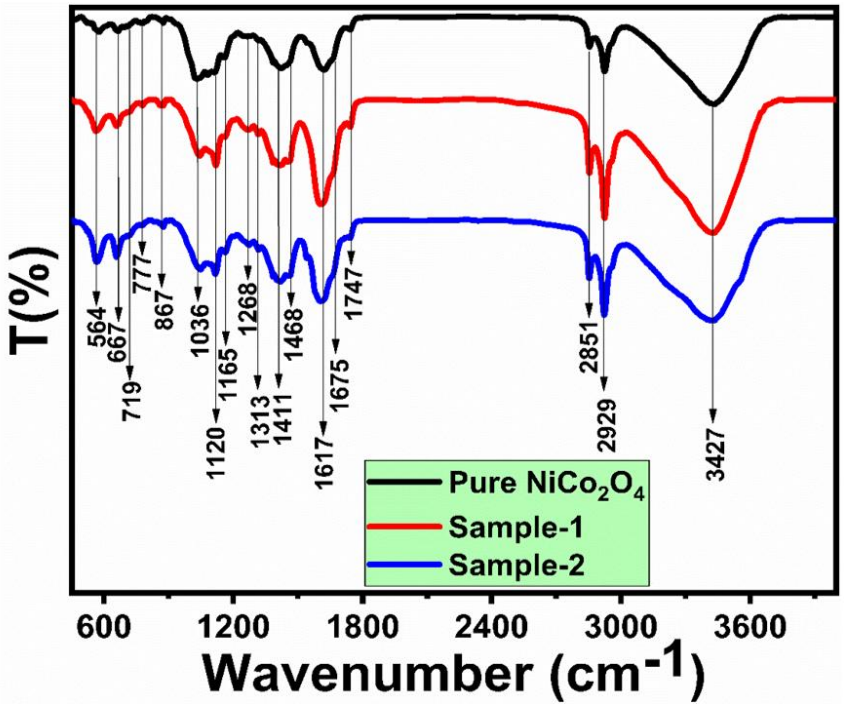

Figure 3. FTIR spectra of pure $NiCo_2O_4$ nanostructures, and PVP assisted $NiCo_2O_4$ nanowires (sample 1 and sample 2).

Figure 4. CV polarization curves of bare GCE (BGCE) and pure $NiCo_2O_4$ nanostructures, PVP assisted $NiCo_2O_4$ nanowires (sample 1 and sample 2) at scan rate of 50 mV/s 0.1M NaOH and in

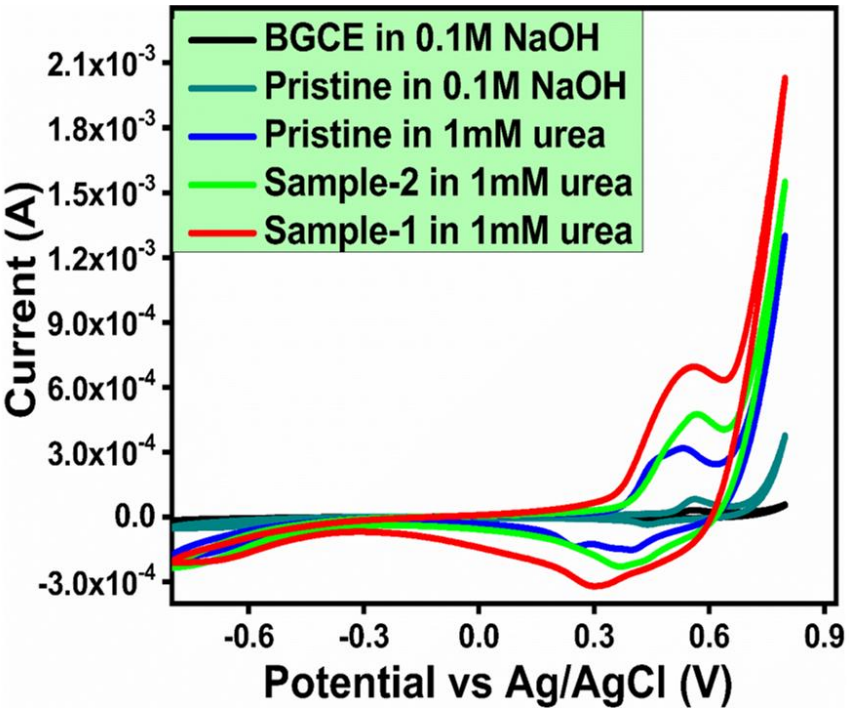

1 mM urea.

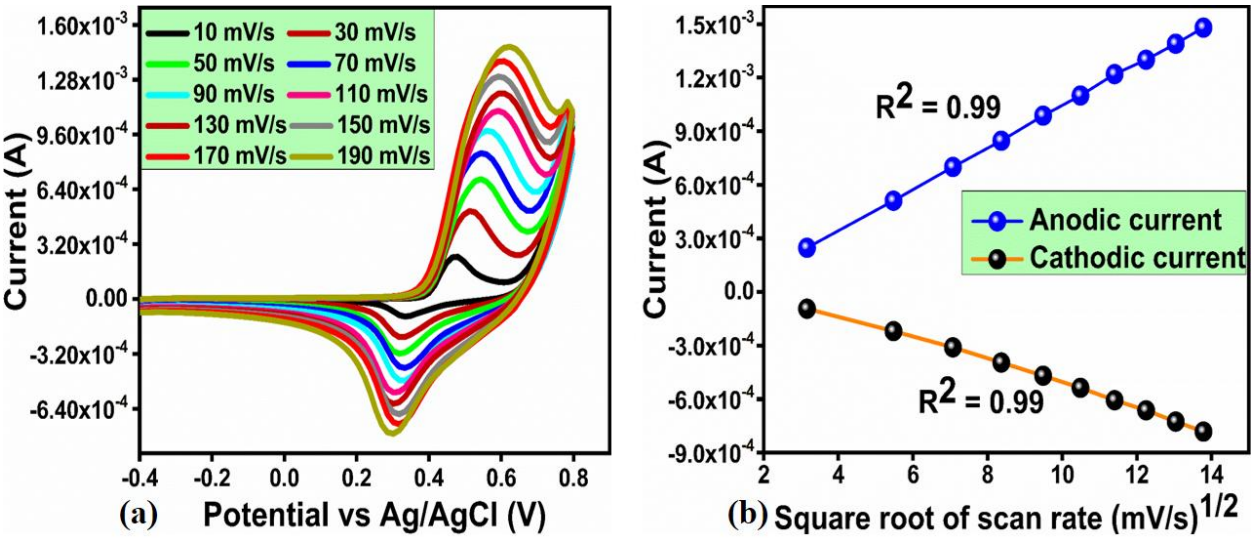

Figure 5: (a) CV cures at different scan rates for PVP assisted $NiCo_2O_4$ nanowires (sample 1) in 1mM urea prepared in 0.1M NaOH, (b) Correspond linear fit of oxidation peak current against square root of scan rate

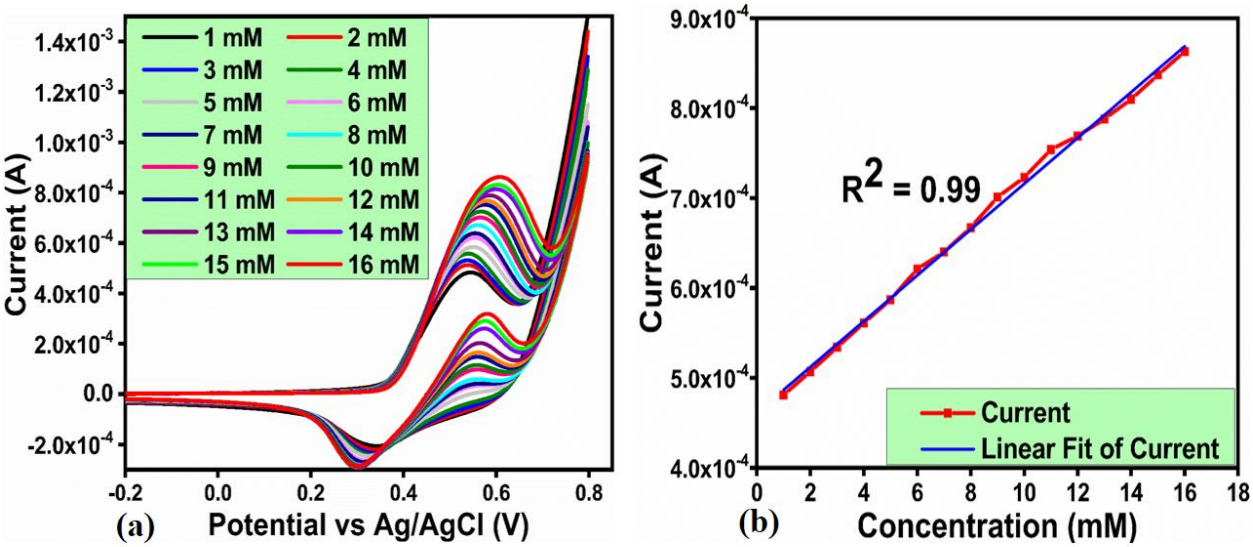

Figure 6: (a) CV curves at scan rate of 50 mV/s of PVP assisted $NiCo_2O_4$ nanowires (sample 1) in different urea concentrations, **(b)** Linear plot of oxidation peak current versus various urea concentrations.

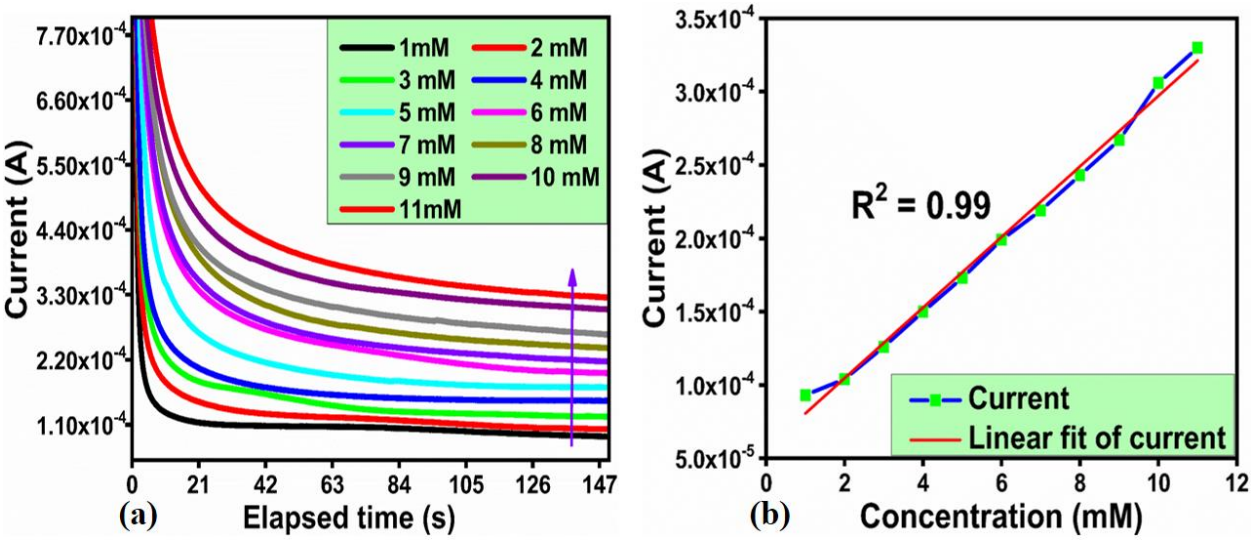

Figure 7: **(a)** Chronoamperometry response time curves of PVP assisted $NiCo_2O_4$ nanowires (sample 1)) in different urea concentrations, **(b)** Linear plot of stable amperometric current versus different urea concentrations.

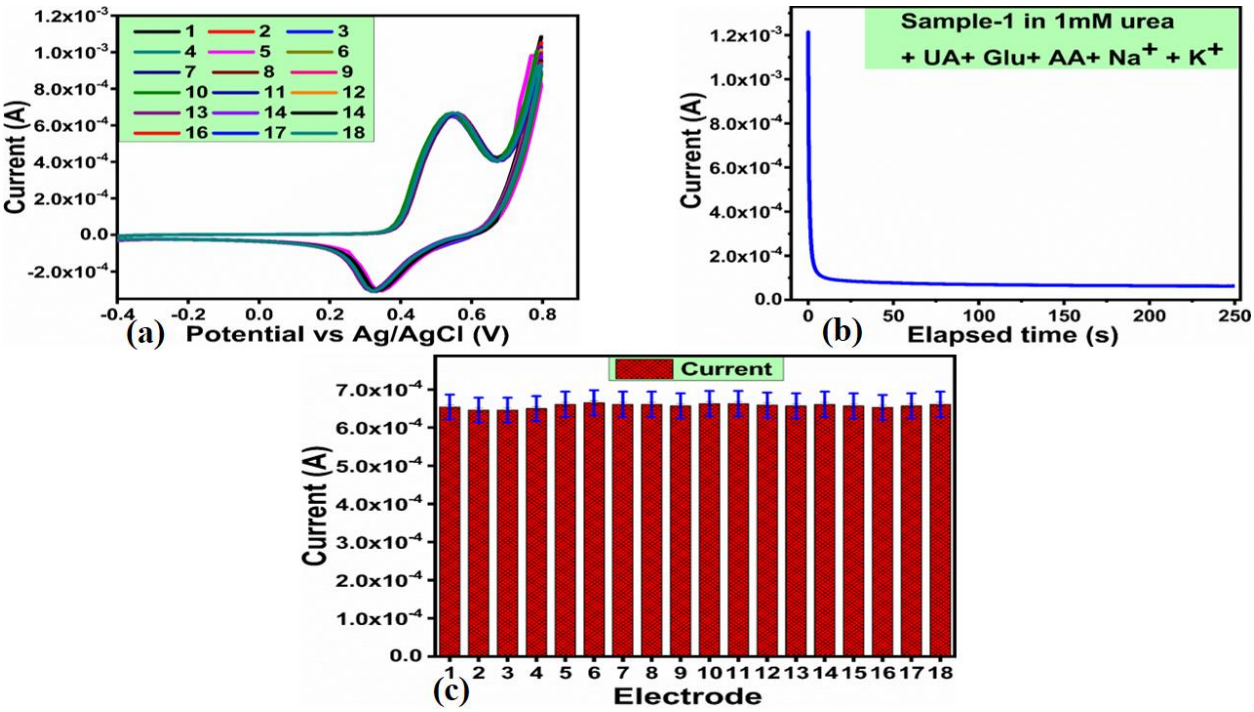

Figure 8: Stability of PVP assisted $NiCo_2O_4$ nanowires (sample 1) in 1mM urea using various repeatable CV cycles at scan rate of 50 mV/s, (b) Selectivity study of PVP assisted $NiCo_2O_4$ nanowires (sample 1) in 1mM and in the presence of 0.1mM concentrations of different interfering agents, (c) Bar graph presentation of variation of oxidation peak current of CV curves shown in Figure 8(a).

5. References

[1]. M.Gerard,A.Chaubey,B.D. Malhotra. Biosens. Bioelectron. 2022**, 17**, 345–359.

[2]. Dhand, C., Das, M., Datta, M. and Malhotra, B.D., 2011. Recent advances in polyaniline based biosensors. Biosensors and Bioelectronics, 26(6), pp.2811-2821.F.S.Wang,D.L. Goh, H.T. Ong, J. Med. Case Rep. 2018, **12**, 1-5.

[3]. Mishra, G.K.; Mishra, R.K.; Bhand, S. Flow injection analysis biosensor for urea analysis in adulterated milk using enzyme thermistor. Biosensors and Bioelectronics, 2010, 26, 1560-1564.

[4]. Sumana, G.; Das, M.; Srivastava, S.; Malhotra, B.D. A novel urea biosensor based on zirconia. Thin Solid Films, 2010, 519, 1187-1191.

[5]. Pizzariello, A.; Stredanský, M.; Stredanská, S.; Miertuš, S. Urea biosensor based on amperometric pH-sensing with hematein as a pH-sensitive redox mediator. Talanta, 2001, 54, 763-772.

[6]. Abbas, M.N.; Magar, H.S. Highly sensitive and selective solid-contact calcium sensor based on Schiff base of benzil with 3-aminosalycilic acid covalently attached to polyacrylic acid amide for health care. Journal of Solid State Electrochemistry, 2018, 22,181-192.

[7]. Abbas, M.N.; Amer, H.S. A solid-contact indium (III) sensor based on a thiosulfinate ionophore derived from omeprazole. Bulletin of the Korean Chemical Society, 2013, 34, 1153-1159.

[8]. Robertson, A.H.; Black, L.A.; Breed, R.S.; Brito, A.D.L.G.; Cowley, R.F.; Gibbard, J. Standard methods for the examination of dairy products. American Journal of Public Health and the Nations Health, 1949, 39, 80-82.

[9]. Bojic, J.; Radovanovic, B.; Dimitrijevic, J. Spectrophotometric determination of urea in dermatologic formulations and cosmetics. Analytical sciences, 2008, 24, 769-774.

[10]. Koebel, M.; Elsener, M. Determination of urea and its thermal decomposition products by high-performance liquid chromatography. Journal of Chromatography A, 1995, 689, 164-169.

[11]. Simeral, L.S. Determination of urea, nitrate, and ammonium in aqueous solution using nitrogen-14 nuclear magnatic resonance. Applied spectroscopy, 1997, 51, 1585-1587.

[12]. Ramsing, A.; Růžička, J.; Hansen, E.H. A new approach to enzymatic assay based on flow-injection spectrophotometry with acid-base indicators. Analytica chimica acta, 1980, 114, 5-181.

[13]. Patton, C.J.; Crouch, S.R. Spectrophotometric and kinetics investigation of the Berthelot reaction for the determination of ammonia. Analytical chemistry, 1977, 49, 464-469.

[14]. Roch-Ramel, F. An enzymic and fluorophotometric method for estimating urea concentrations in nanoliter specimens. Analytical biochemistry, 1967, 21, 372-381.

[15]. Boubriak, O.A.; Soldatkin, A.P.; Starodub, N.F.; Sandrovsky, A.K.; El'skaya, A.K. Determination of urea in blood serum by a urease biosensor based on an ion-sensitive field-effect transistor. Sensors and Actuators B: Chemical, 1995, 27, 429-431.

[16]. Bobacka, J.; Ivaska, A.; Lewenstam, A. Potentiometric ion sensors based on conducting polymers. Electroanalysis: An International Journal Devoted to Fundamental and Practical Aspects of Electroanalysis, 2003, 15, 366-374.

[17]. Hassan, R.Y. Advances in electrochemical nano-biosensors for biomedical and environmental applications: From current work to future perspectives. Sensors, 2022, 22, 7539.

[18]. Arafa, K.K.; Ibrahim, A.; Mergawy, R.; El-Sherbiny, I.M.; Febbraio, F.; Hassan, R.Y. Advances in cancer diagnosis: Bio-electrochemical and biophysical characterizations of cancer cells. Micromachines, 2022, **13**, 1401-17.

[19]. El-Fatah, G.A.; Magar, H.S.; Hassan, R.Y.; Mahmoud, R.; Farghali, A.A.; Hassouna, M.E. A novel gallium oxide nanoparticles-based sensor for the simultaneous electrochemical detection of Pb2+, Cd2+ and Hg2+ ions in real water samples. Scientific Reports, 2022, **12**, 20181.

[20]. Magar, H.S.; Ghica, M.E.; Abbas, M.N.; Brett, C.M.Highly sensitive choline oxidase enzyme inhibition biosensor for lead ions based on multiwalled carbon nanotube modified glassy carbon electrodes. Electroanalysis, 2017, **29**, 1741–1748.

[21]. Abbas, M.N.; Amer, H.S. A solid-contact indium (III) sensor based on a thiosulfinate ionophore derived from omeprazole. Bulletin of the Korean Chemical Society,2013**, 34**, 1153–1159.

[22]. Abbas, M.N.; Amer, H.S. A novel solid-contact sensor for flow injection determination of verapamil in pharmaceutical formulations and urine. Current Pharmaceutical Analysis,2008, **4**, 90–100.

[23]. H Magar, H.S.; Brahman, P.K.; Hassan, R.Y. Disposable impedimetric nano-immunochips for the early and rapid diagnosis of Vitamin-D deficiency. Biosensors and Bioelectronics: X, 2022, **10,** 100124.

[24]. Magar, H.S.; Ghica, M.E.; Abbas, M.N.; Brett, C.M. A novel sensitive amperometric choline biosensor based on multiwalled carbon nanotubes and gold nanoparticles. Talanta2017, **167**, 462–469.

[25]. Kirsch, J.; Siltanen, C.; Zhou, Q.; Revzin, A.; Simonian, A. Biosensor technology: recent advances in threat agent detection and medicine. Chemical Society Reviews2013, **42,** 8733–8768.

[26]. Castillo, J.; Gáspár, S.; Leth, S.; Niculescu, M.;Mortari, A.; Bontidean, I.; Soukharev, V.; Dorneanu, S.A.; Ryabov, A.D.; Csöregi, E. Biosensors for life quality: Design, development and applications. Sensors and Actuators B: Chemical,2004, **102,** 179–194.

[27]. Grieshaber, D.; MacKenzie, R.; Vörös, J.; Reimhult, E. Electrochemical biosensors-sensor principles and architectures. Sensors,2008, **8,** 1400–1458.

[28]. Tohamy, H.A.S.; Magar, H.S. A flexible, low-cost, disposable non-enzymatic electrochemical sensor based on MnO2/Cellulose nanostructure. ECS Journal of Solid State Science and Technology,2022, **11,** 127003.

[29]. Naresh, V.; Lee, N. A review on biosensors and recent development of nanostructured materials-enabled biosensors. Sensors, 2021, **21,** 1109

[30]. Chang, A.S.; Tahira, A.; Chang, F.; Solangi, A.G.; Bhatti, M.A.; Vigolo, B.; Nafady, A.; Ibupoto, Z.H. Highly heterogeneous morphology of cobalt oxide nanostructures for the development of sensitive and selective ascorbic acid non-enzymatic sensor. Biosensors, 2023, **13**, 147-63.

[31]. Keating, C.D.; Natan, M.J. Striped metal nanowires as building blocks and optical tags. *Advanced Materials*, 2003, ***15***, 451-454.

[32]. Mirkovic, T.; Zacharia, N.S.; Scholes, G.D.; Ozin, G.A. Nanolocomotion—catalytic nanomotors and nanorotors. *small*, 2010, ***6***, 159-167.

[33]. Wang, Y.; Fei, S.T.; Byun, Y.M.; Lammert, P.E.; Crespi, V.H.; Sen, A.; Mallouk, T.E. Dynamic interactions between fast microscale rotors. *Journal of the American Chemical Society*, 2009, ***131***, 9926-9927.

[34]. Wu, J.; Balasubramanian, S.; Kagan, D.; Manesh, K.M.; Campuzano, S.; Wang, J. Motion-based DNA detection using catalytic nanomotors. *Nature Communications*, 2010, ***1***, 36.

[35]. Gao, W.; Pei, A.; Wang, J.; Water-driven micromotors. *ACS nano*, 2012, ***6***, 8432-8438.

[36]. Paxton, W.F.; Kistler, K.C.; Olmeda, C.C.; Sen, A.; St. Angelo, S.K.; Cao, Y.; Mallouk, T.E.; Lammert, P.E.; Crespi, V.H. Catalytic nanomotors: autonomous movement of striped nanorods. *Journal of the American Chemical Society*, 2004, ***126***, 13424-13431.

[37]. Chang, A.S.; Tahira, A.; Solangi, Z.A.; Solangi, A.G.; Ibupoto, M.H.; Chang, F.; Medany, S.S.; Nafady, A.; Kasry, A.; Willander, M.; Ibupoto, Z.H. Pd-Co3O4-based nanostructures for the development of enzyme-free glucose sensor. Bulletin of Materials Science,2022, **45,** 62-76.

[38]. Ansari, S.G.; Fouad, H.; Shin, H.S.; Ansari, Z.A. Electrochemical enzyme-less urea sensor based on nano-tin oxide synthesized by hydrothermal technique. Chemico-biological interactions, 2015, **242**, 45–49.

[39]. Amin, S.; Tahira, A.; Solangi, A.; Beni, V.; Morante, J.R.; Liu, X.; Falhman, M.; Mazzaro, R.; Ibupoto, Z.H.; Vomiero, A. A practical non-enzymatic urea sensor based on NiCo 2 O 4 nanoneedles. RSC advances, 2019, **9**, 14443–14451.

[40]. Nguyen, N.S.; Das, G.; Yoon, H.H. Nickel/cobalt oxide-decorated 3D graphene nanocomposite electrode for enhanced electrochemical detection of urea. Biosensors and Bioelectronics, 2016, **77,** 372–377.

[41]. Mondal, S.; Sangaranarayanan, M.V. A novel non-enzymatic sensor for urea using a polypyrrole-coated platinum electrode. Sensors and Actuators B: Chemical, 2013, **177**, 478–486.

[42]. Hassanpoor, S.; Aghely, F. Hierarchically self-assembled NiCo 2 O 4 nanopins as a high-performance supercapacitor cathodic material: A morphology controlled study. RSC advances, 2020, **10**, 35235–35244.

[43]. Yu, Z.; Li, H.; Zhang, X.; Liu, N.; Tan, W.; Zhang, X.; Zhang, L. Facile synthesis of NiCo2O4@ Polyaniline core–shell nanocomposite for sensitive determination of glucose. Biosensors and Bioelectronics, 2016, **75**, 161–165.

[44]. Zhan, J.; Cai, M.; Zhang, C.; Wang, C. Synthesis of mesoporous NiCo2O4 fibers and their electrocatalytic activity on direct oxidation of ethanol in alkaline media. Electrochimica Acta, 2015, **154**, 70–76.

[45]. Yu, H.; Jin, J.; Jian, X.; Wang, Y.; Qi, G.C. Preparation of cobalt oxide nanoclusters/overoxidized polypyrrole composite film modified electrode and its application in nonenzymatic glucose sensing. Electroanalysis, 2013, **25**, 1665–1674.

[46]. Pasta, M.; La Mantia, F.; Cui, Y. Mechanism of glucose electrochemical oxidation on gold surface. Electrochimica Acta, 2010, **55,** 5561–5568.

[47]. Raghuram, N.; Rao, T.S.; Naidu, K.C.B. Electrical and impedance spectroscopy properties of hydrothermally synthesized Ba0. 2Sr0. 8-yLayFe12O19 (y= 0.2–0.8) nanorods. Ceramics International, **2020, 46**, 5894-5906.

[48]. Raghuram, N.; Rao, T.S.; Naidu, K.C.B. Magnetic properties of hydrothermally synthesized Ba 1–x Sr x Fe 12 O 19 (x= 0.0–0.8) nanomaterials. Applied Physics A, 2019**, 125,** 839

[49]. Zhang, J.; Sun, Y.; Li, X.; Xu, J. Fabrication of NiCo2O4 nanobelt by a chemical co-precipitation method for non-enzymatic glucose electrochemical sensor application. Journal of Alloys and Compounds, 2020**, 831**, 154796

[50]. Wang, D.; Mukhtar, A.; Humayun, M.; Wu, K.; Du, Z.; Wang, S.; Zhang, Y. A Critical Review on Nanowire-Motors: Design, Mechanism and Applications. *The Chemical Record*, 2022, **22**, e202200016.

[51]. Wang, D.S.; Mukhtar, A.; Wu, K.M.; Gu, L.; Cao, X. Multi-segmented nanowires: a high tech bright future. *Materials*, 2019, **23**, 3908.

[52]. Wang, D.; Hu, Y.; Cui, Z.; Yang, P.; Du, Z.; Hou, Y.; Yang, P.; Rao, J.; Wang, C.; Zhang, Y. Sulfur vacancy regulation and multipolarization of NixCo1S nanowires-decorated biotemplated structures to promote microwave absorption. *Journal of Colloid and Interface Science*, 2023, ***646***, 991-1001.

[53]. Wang, D.; Yang, P.; Hu, Y.; Cui, Z.; Du, Z.; Yang, P.; Yi, S.; Rao, J.; Zhang, Y. 1D-3D biological template loaded NiCo nanowires at high temperatures as a broadband, lightweight electromagnetic wave absorbing material. *Powder Technology*, 2023, **426**, 118670.

[54]. Zhang, C.; Wang, D.; Dong, L.; Li, K.; Zhang, Y.; Yang, P.; Yi, S.; Dai, X.; Yin, C.; Du, Z.; Zhang, X. Microwave Absorption of α-Fe2O3@ diatomite Composites. *International Journal of Molecular Sciences*, 2022, **23**, 9362.

[55]. Du, Z.; Wang, D.; Zhang, X.; Yi, Z.; Tang, J.; Yang, P.; Cai, R.; Yi, S.; Rao, J.; Zhang, Y. Core-Shell Structured SiO2@ NiFe LDH Composite for Broadband Electromagnetic Wave Absorption. *International Journal of Molecular Sciences*, 2022, **24**, 504.

[56]. Nasrinpour, H.; Masoudpanah, S.M.; Soltanieh, M.Oxalate-assisted solvothermal synthesis of octahedral LiMn1. 5Ni0. 5O4 particles for lithium-ion batteries. Journal of Materials Research and Technology 2021, **13**, 61-69.

[57]. Park, J.; Jo, S.; Kitchamsetti, N.; Zaman, S.; Kim, D. The development of NiCo2O4/PVP/PANI heterogeneous nanocomposites as an advanced battery-type electrode material for high-performing supercapacitor application. Journal of Alloys and Compounds, 2022**, 926**,166815.

[58]. Fu, H.; Liu, Y.; Chen, L.; Shi, Y.; Kong, W.; Hou, J.; Yu, F.; Wei, T.; Wang, H.; Guo, X. Designed formation of NiCo2O4 with different morphologies self-assembled from nanoparticles for asymmetric supercapacitors and electrocatalysts for oxygen evolution reaction. Electrochimica Acta, 296, pp.719-729

[59]. Chand, P.; Joshi, A.; Lal, S.; Singh, V. Effect of hydrothermal temperature on structural, optical and electrochemical properties of α-MnO2 nanostructures for supercapacitor application. Chemical Physics Letters, 777, p.138742.

[60]. Yang, M.; Bai, Q.; Ding, C. NiMoO4 nanoparticles embedded in nanoporous carbon nanosheets derived from peanut shells: Efficient electrocatalysts for urea oxidation. Colloids and Surfaces A: Physicochemical and Engineering Aspects, 2020**, 604**,125276.

[61]. Sivakumar, P.; Ramesh, R.; Ramanand, A.; Ponnusamy, S.; Muthamizhchelvan, C. Synthesis and characterization of NiFe2O4 nanosheet via polymer assisted co-precipitation method. *Materials Letters*, 2011, ***65***, 483-485.

[62]. Koebel, M.M.; Jones, L.C.; Somorjai, G.A. Preparation of size-tunable, highly monodisperse PVP-protected Pt-nanoparticles by seed-mediated growth. *Journal of Nanoparticle Research*, 2008, ***10***, 1063-1069.

[63]. Roosen, A.R.; Carter, W.C. Simulations of microstructural evolution: anisotropic growth and coarsening. *Physica A: Statistical Mechanics and Its Applications*, 1998, ***261***(1-2), 232-247.

[64]. Ghosh, G.; Naskar, M.K.; Patra, A.; Chatterjee, M. Synthesis and characterization of PVP-encapsulated ZnS nanoparticles. *Optical Materials*, 2006, ***28*** (8-9), 1047-1053.

[65]. Shao, H.; Huang, Y.; Lee, H.; Suh, Y.J.; Kim, C.O. Effect of PVP on the morphology of cobalt nanoparticles prepared by thermal decomposition of cobalt acetate. *Current Applied Physics*, 2006, ***6***, e195-e197.

[66]. Huang, W.Y.; Xu, G.C. Characterization of nano-Ag/PVP composites synthesized via ultra-violet irradiation. *Journal of Coal Science and Engineering (China)*, 2010, ***16***, 188-192.

[67]. Tsuji, M.; Hashimoto, M.; Nishizawa, Y.; Tsuji, T. Synthesis of gold nanorods and nanowires by a microwave–polyol method. *Materials Letters*, 2004, ***58*** (17-18), 2326-2330.

[68]. Goodarz Naseri, M.; Saion, E.; Khalil Zadeh, N. The amazing effects and role of PVP on the crystallinity, phase composition and morphology of nickel ferrite nanoparticles prepared by thermal treatment method. *International nano letters*, 2013, ***3***,1-8.

---

[69]. Naik, T.S.K.; Saravanan, S.; Saravana, K.S.; Pratiush, U.; Ramamurthy, P.C. A non-enzymatic urea sensor based on the nickel sulfide/graphene oxide modified glassy carbon electrode. Materials Chemistry and Physics, 2020, **245,** 122798.

[70]. Arain, M.; Nafady, A.; Ibupoto, Z.H.; Sherazi, S.T.H.;Shaikh, T.; Khan, H.; Alsalme, A.; Niaz, A.; Willander, M. Simpler and highly sensitive enzyme-free sensing of urea via NiO nanostructures modified electrode. RSC advances, 2016, 6, 39001-39006.

---

[71]. Nia, S.M.; Kheiri, F.; Jannatdoust, E.; Sirousazar, M.; Chianeh, V.A.; Kheiri, G. A Highly Sensitive Non-Enzymatic Urea Sensor Based on Ni (OH)2/Mn3O4/rGO/PANi Nanocomposites Using Screen-Printed Electrodes. J. Electrochem. Soc. 2021, 168, 067504

[72]. Salarizadeh, N.; Habibi-Rezaei, M.; Zargar, S.J. NiO–MoO3 nanocomposite: A sensitive non-enzymatic sensor for glucose and urea monitoring. Mater. Chem. Phys. 2022, 281, 125870.

[73]. Bao, C.; Niu, Q.; Chen, Z.-A.; Cao, X.; Wang, H.; Lu, W. Ultrathin nickel-metal–organic framework nanobelt based electrochemical sensor for the determination of urea in human body fluids. RSC Adv. 2019, 9, 29474–29481

[74]. Kumar, T.V.; Sundramoorthy, A.K. Non-enzymatic electrochemical detection of urea on silver nanoparticles anchored nitrogendoped single-walled carbon nanotube modified electrode. J. Electrochem. Soc. 2018, 165, B3006.

[75]. Farithkhan, A.; John, S.A. Three-Dimensional Coral-Like NiFe-Layered Double Hydroxides on Biomass-Derived Nitrogen-Doped Carbonized Wood as a Sensitive Probe for Nonenzymatic Urea Determination. ACS Sustain. Chem. Eng. 2022, 10, 6952–6962.